

## Spin filtering in nanowire directional coupler

M. Rebello Sousa Dias,<sup>1,2,3</sup> V. Lopez-Richard,<sup>1</sup> G. E. Marques,<sup>1</sup> and S. E. Ulloa<sup>2,3</sup>

<sup>1)</sup>*Departamento de Física, Universidade Federal de São Carlos, 13565-905, São Carlos, São Paulo, Brazil*

<sup>2)</sup>*Department of Physics and Astronomy and Nanoscale and Quantum Phenomena Institute, Ohio University, Athens, Ohio 45701-2979*

<sup>3)</sup>*Dahlem Center for Complex Quantum Systems and Fachbereich Physik, Freie Universität Berlin, 14195 Berlin, Germany*

The spin transport characteristics of a nanowire directional electronic coupler have been evaluated theoretically via a transfer matrix approach. The application of a gate field in the region of mixing allows for control of spin current through the different leads of the coupler via the Rashba spin-orbit interaction. The combination of spin-orbit interaction and applied gate voltages on different legs of the coupler give rise to a controllable modulation of the spin polarization. Both structural factors and field strength tuning lead to a rich phenomenology that could be exploited in spintronic devices.

The nature of electron and spin transport mechanisms can be unveiled by exploring the properties of coupled nanowires (NW). The realization of a directional coupler gave rise, through proximity and tunneling effects,<sup>1,2</sup> to the modulation of quantum transport in a phase-coherent system.<sup>3</sup> The spin modulation in a single NW via spin-orbit interaction (SOI) has been proposed<sup>4</sup> and refined<sup>5–9</sup> to achieve a spin-orbit quantum bit device.<sup>10</sup> More recently, SOI in semiconductor NWs has enabled the possible observation and characterization of Majorana fermions.<sup>11–14</sup> Exploring all-electrical spin transport has motivated a search for new configurations of nanostructures<sup>15–18</sup> and a wave guide directional coupler appears as a promising device geometry.

In this work, we study the spin transport properties of parallel NWs, in a directional “H-shape” coupler geometry, connected through a region of the same material but locally gated, Fig. 1(a). The application of a gate field ( $\mathbf{E}$ ) in the connecting region generates a Rashba SOI, which breaks spin degeneracy,<sup>19</sup> Fig. 1(b). While the Rashba field does not break time reversal symmetry, the symmetries of the configuration impose additional constraints on the transport characteristics.<sup>9,18,20</sup>

We find that, while being able to control the electronic flux through the different wires across the mixing region, as expected, it is also possible to electrically control the *spin flux* across the device, whenever spin-polarized injection is considered. Moreover, we find that there is a net spin-polarized flux perpendicular to the current, which can be controlled by the gate potential in the mixing region, as well as by local gates at the NWs. This overall control of charge and spin flux in a directional coupler appears promising for spintronics, as well as in hybrid devices composite with superconducting or magnetic materials.

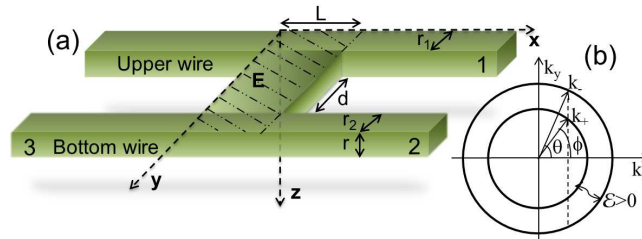


FIG. 1. (a) Scheme of nanowire (NW) directional coupler with two parallel NW’s connected in the middle region by the same material. The  $z$ -thickness of the entire region is  $r$ ,  $r_1$  is the  $y$ -width of the upper wire,  $r_2$  of the bottom wire,  $d$  is the NW separation,  $L$  is the length of the mixing region, and  $\mathbf{E}$  is the electric field along the  $z$ -direction generated by the local gate in the shaded central region. (b) Spectrum of 2DEG with Rashba SOI at fixed energy  $\mathcal{E}$ . For propagation with positive fixed  $x$ -component one has four possible values of  $k_y$  ( $\pm k_- \sin \theta$ , and  $\pm k_+ \sin \phi$ ), as indicated.

The transfer matrix method<sup>21</sup> was used to calculate the transport characteristics of the system. The single-particle Hamiltonian with  $xy$ -plane dynamics has the form

$$\hat{H} = \frac{\hat{\mathbf{p}}^2}{2m} + V_c(y, z) + \frac{1}{2\hbar}[\alpha(\mathbf{r}) \cdot (\sigma_x \hat{p}_y - \sigma_y \hat{p}_x)], \quad (1)$$

where  $\hat{p}_i = -i\hbar\nabla_i$ ,  $\sigma_i$  are the Pauli matrices,  $\alpha(\mathbf{r})$  is the Rashba SOI interaction (proportional to the gate field  $\mathbf{E}$ ), and  $V_c(y, z)$  is the hard wall confinement potential in the  $y$ - and  $z$ -direction. The eigenfunctions for the Hamiltonian (1), for vanishing  $\alpha(\mathbf{r})$ , in the NWs with square cross section are given by

$$|\phi_j^\sigma\rangle = \sqrt{\frac{2}{r_{1,2}}} \sin\left(\frac{n_y \pi y}{r_{1,2}}\right) \sqrt{\frac{2}{r}} \sin\left(\frac{n_z \pi z}{r}\right) e^{ik_x x} |\sigma\rangle, \quad (2)$$

with corresponding eigenvalues

$$\mathcal{E}_{k_x, n_y, n_z, \sigma}^0 = \frac{\hbar^2}{2m} \left( k_x^2 + \frac{\pi^2 n_y^2}{r_{1,2}^2} + \frac{\pi^2 n_z^2}{r^2} \right). \quad (3)$$

The index  $j$  refers to each wire branch:  $j = 1$  corresponds to the upper wire on the right side;  $j = 2$  to the bottom right wire; and  $j = 3$  to the bottom left wire (see Fig. 1(a)). Also,  $|\sigma\rangle$  indicates the spinor, and  $n_y$  and  $n_z$  are quantum numbers for the lateral and vertical confinement, respectively. For simplicity, we consider  $n_z = 1$  and two transport channels,  $n_y = 1, 2$ .

Treating the intermediate mixing region with SOI perturbatively, where  $\alpha(\mathbf{r}) \neq 0$ , the first order correction is dominated by the intrasubband terms ( $n_y = n'_y$ ),  $\langle \phi' | \alpha \hat{H}_1 | \phi \rangle \simeq -\frac{i}{2} \alpha k_x \sigma \delta_{\sigma', -\sigma}$ , where,  $\sigma, \sigma' = \pm 1$ , for spin up and down, respectively. This gives rise to the eigenvalue equation,

$$\begin{pmatrix} 0 & \frac{i\alpha k_x}{2} \\ \frac{-i\alpha k_x}{2} & 0 \end{pmatrix} \begin{pmatrix} C^\uparrow \\ C^\downarrow \end{pmatrix} = \mathcal{E}^{(1)} \begin{pmatrix} C^\uparrow \\ C^\downarrow \end{pmatrix}, \quad (4)$$

which gives the first order correction to the energy levels  $\mathcal{E}_\pm^{(1)} = \pm \frac{\alpha k_x}{2}$ , and respective eigenvectors

$$|\psi_n^\sigma\rangle_\pm = \frac{1}{\sqrt{2}} \left[ |\phi_n^\sigma\rangle \pm i |\phi_n^{-\sigma}\rangle \right]. \quad (5)$$

Hence, the wave number component in the  $x$ -direction for a given energy  $\mathcal{E}$  can be written in the mixing region as

$$k_n^\pm = \sqrt{\frac{2m\mathcal{E}}{\hbar^2} - \frac{\pi^2 n^2}{(d + r_1 + r_2)^2} - \frac{\pi^2}{r^2} + \frac{\alpha^2 m^2}{4\hbar^4}} \mp \frac{\alpha m}{2\hbar^2}. \quad (6)$$

For the transfer matrix calculation the system is divided into three regions: the regions where  $x < 0$  (left) and  $x > L$  (right) with no SOI ( $\alpha = 0$ ), and  $0 < x < L$  (middle region) with SOI ( $\alpha \neq 0$ ), as depicted in Fig. 1. The interface between these regions is considered sharp for simplicity, and the boundary conditions result in the relations<sup>22</sup>

$$\begin{aligned} \frac{\partial \Psi(\epsilon_0)}{\partial x} + \frac{m i \sigma_y}{\hbar^2} \alpha(\epsilon_0) \Psi(\epsilon_0) = \\ \frac{\partial \Psi(-\epsilon_0)}{\partial x} + \frac{m i \sigma_y}{\hbar^2} \alpha(-\epsilon_0) \Psi(-\epsilon_0), \end{aligned} \quad (7)$$

where the mass is assumed to be the same everywhere, and  $\epsilon_0 \rightarrow 0$  or  $L$  at the two interfaces. An  $8 \times 8$  transfer matrix is built relating the coefficients (incident, transmitted, and reflected waves for spin up and down) for a given incident spin, for the bottom and upper wires

$$\begin{pmatrix} \mathbf{I} \\ \mathbf{R} \end{pmatrix} = \mathbf{M}_{\text{Left}}(0)^{-1} \mathbf{M}_{\text{Middle}}(0) \times \mathbf{M}_{\text{Middle}}(L)^{-1} \mathbf{M}_{\text{Right}}(L) \begin{pmatrix} \mathbf{T} \\ \mathbf{I}' \end{pmatrix}, \quad (8)$$

where  $\mathbf{T} = T_j^{\sigma'\sigma}$ ,  $\mathbf{R} = R_j^{\sigma'\sigma}$ , and  $\mathbf{I}' = I_j^{\sigma'\sigma}$  are all four dimensional vectors for the transmitted, reflected, and incident amplitudes for the different NW branches, with incident spin  $\sigma'$ , and outgoing spin  $\sigma$ . The overlap terms, which contain information on the geometry and lateral confinement are included in the matrices  $\mathbf{M}_{\text{Middle}}(0)$  and  $\mathbf{M}_{\text{Middle}}(L)$ .

The quantum transport properties of interconnected parallel wires through a potential barrier<sup>1,3,23,24</sup> can be controlled by changing the barrier height and length. Similarly, one can modulate the carrier and spin transport by varying the length  $L$  of the middle mixing region and the separation  $d$  between wires. The formalism enables the study of different spin polarization configurations for the incident waves. We present results for an incident wave in one of the wires with up or down spin-polarization along the  $z$ -direction. The transmission and reflection amplitudes (the entire scattering matrix) will be shown below to exhibit oscillations arising from the expected interference among the various channels, as they mix in the coupling region. This interference has characteristic energy (or length) scales associated with the different components producing the interference. We will also see that the onset of spin-orbit coupling in the mixing region further complicates the pattern of oscillations, as SOI effectively duplicates the number of available channels at a given energy.

Figure 2 shows the transmission and reflection coefficients vs the length of mixing region  $L$  for an incident spin-down polarized wave (inset Fig. 2), where  $d = 100$  Å, and  $r_1 =$

$r_2 = 100$  Å. We can see in Fig. 2(d) that the spin-preserving transport coefficient  $T_2^{\uparrow\downarrow}$  can be suppressed or enhanced with a characteristic periodicity  $\simeq L_{\Delta k} = 2\pi/\Delta k$ . For a given incident energy  $\mathcal{E}$ , there are corresponding wave vectors  $k_n^\pm$  along each given channel,  $n = 1, 2$  (Eq. (6)). The momentum difference  $\Delta k = k_1^\sigma - k_2^\sigma$ , is responsible for the long period oscillations as the two ( $\pm$ ) channels interfere with one another. For  $\mathcal{E} = 50$  meV, one finds  $L_{\Delta k} = 2\pi/\Delta k \simeq 120$  nm, a value that coincides with the oscillation period. Moreover, whenever  $T_2^{\sigma'\sigma}$  is enhanced,  $T_1^{\sigma'\sigma}$  is suppressed (Fig. 2(b) and (d))—i.e, they oscillate out of phase, illustrating their competition. Opposite phase oscillations between the NWs result for a symmetric system such as this, where the initial conditions have the incident wave in only one of the coupled NW's (inset Fig. 2). The coefficients also show fast oscillations characterized by  $L_{\mathcal{E}} = \sqrt{\pi^2 \hbar^2 / 2m\mathcal{E}}$ , in analogy with the quantum well system. For  $\mathcal{E} = 50$  meV, these fast oscillations have the corresponding length scale  $L_{\mathcal{E}} \simeq 10$  nm. Thus, one is able to adjust the transmission by changing sizes, widths, and lengths of mixing regions, as expected from the directional coupler geometry of the system.<sup>1,2,23</sup>

The introduction of SOI provides additional control on the overall transmission amplitudes, as well as on the spin polarized transmission. The SOI length scale, given by the period over which the spin precesses from  $\uparrow$  to  $\downarrow$  (and vice versa) due to the effective Rashba field, is  $L_{SO} = \pi \hbar^2 / \alpha m$  ( $\simeq 230$  nm, in Fig. 2). One can clearly see the effect of this precession in Fig. 2(b), where the incident spin down is fully transmitted in the up-projection at  $L \simeq L_{SO}$ ,  $T_1^{\uparrow\uparrow}$ , while the spin-preserving channel is nearly fully blocked,  $T_1^{\uparrow\downarrow} \simeq 0$ . Figure 2(a) and (c) show the reflection ( $R^{\downarrow\sigma}$ ) and transmission in the bottom wire on the left NW ( $T_3^{\downarrow\sigma}$ ), respectively. These coefficients are characterized by oscillations with shorter periods due to the fact that the wave travels twice the distance  $L$ . Moreover, in this configuration the length scale  $L_{SO}$  becomes comparable to  $2L_{\Delta k}$ , resulting in a more complex interference and the beating behavior evident on  $R^{\downarrow\downarrow}$ . These results are for a spin-polarized incident wave; reversing the incident spin produces the spin reversal of the transmitted and reflected amplitudes, as expected from the time-reversal invariance of the Hamiltonian, as well as from the spatial symmetries of the system.<sup>9,18</sup>

To better characterize how the system responds to the injection of a spin unpolarized superposition of spin-up and spin-down fluxes, we calculate the spin persistence ratio  $C_j \equiv [T_j^{\uparrow\uparrow} + T_j^{\downarrow\downarrow} - (T_j^{\downarrow\uparrow} + T_j^{\uparrow\downarrow})] / T$ , where  $T = T_j^{\uparrow\uparrow} + T_j^{\downarrow\downarrow} + T_j^{\downarrow\uparrow} + T_j^{\uparrow\downarrow}$ , for each NW  $j$ . Note that if  $T_j^{\uparrow\uparrow} = T_j^{\uparrow\downarrow}$  and  $T_j^{\downarrow\downarrow} = T_j^{\downarrow\uparrow}$  then  $C_j = 0$ , a signature of a “memoryless” channel; on the

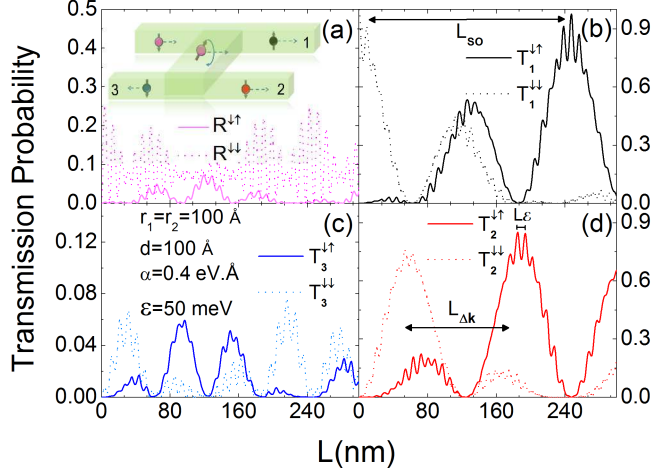


FIG. 2. Transmission probabilities vs length of the mixing region  $L$  for incident spin-down polarized flux ( $I^{\downarrow}$ ), where  $r_1 = r_2 = 100 \text{ \AA}$ ,  $d = 100 \text{ \AA}$ ,  $\mathcal{E} = 50 \text{ meV}$ ,  $\alpha = 0.4 \text{ eV}\cdot\text{\AA}$ , and  $m = 0.026m_0$ . (a) Reflection on the left top wire ( $R^{\downarrow\sigma}$ ). (b) Transmission on the right top wire ( $T_1^{\downarrow\sigma}$ ). (c) Transmission on the left bottom wire ( $T_3^{\downarrow\sigma}$ ). (d) Transmission on the right bottom wire ( $T_2^{\downarrow\sigma}$ ). Notice reflection values in (a) and (c) are much smaller than the transmission in (b) and (d).

other hand,  $C_j = 1$  ( $-1$ ) for a full spin-preserving (or reversing) channel. Figure 3 shows the color map of characteristic  $C_j$  vs  $\alpha$  and  $L$  for each wire branch,  $j$ . The spin reversing regions are identified by the dark (blue) color and evolve with both  $\alpha$  and length  $L$ , such that  $\alpha L \simeq L/L_{SO} = \text{constant}$ , as expected from the Rashba precession length. Alternatively, pale gray regions indicate spin-preserving characteristics. One can also identify nearly  $\alpha$ -independent oscillations, more visible on Fig. 3(a) and (c) within this area, associated with  $L/L_{\Delta k} = \text{constant}$ .

One cannot expect a net spin polarization for the current, even when the system symmetry is broken by applying a gate voltage difference between the wires or making the device asymmetric in other ways. This is due to the fact that for transport along the  $x$ -direction, the electric field on the  $z$ -direction, and corresponding Rashba SOI, will produce spin precession of the  $z$ -spin for both spin components in a symmetric fashion.<sup>18,25</sup> The degree of spin polarization is defined by  $P_j \equiv [T_j^{\uparrow\uparrow} + T_j^{\downarrow\uparrow} - (T_j^{\downarrow\downarrow} + T_j^{\uparrow\downarrow})]/T$ . As expected, there is no net polarization in the  $z$ -direction. However, the effective Rashba magnetic field is along the  $y$ -direction, which suggests one to explore the possibility of tuning this quantity along that axis,  $P_j^y$ . The application of a gate voltage in one of the branches to raise the local energy of the subbands, as well as the strength of the Rashba SOI, can further help to tune the polarization in the remaining output wires. Figure 4 shows  $P_j^y$  as a function of the Rashba

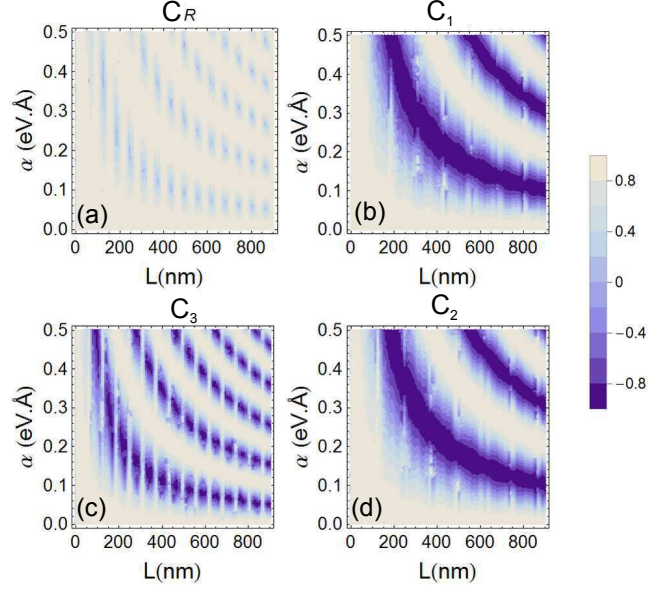


FIG. 3. Map of spin persistence ratio  $C_j$  vs  $\alpha$  and  $L$ , where  $r_1 = r_2 = 100 \text{ \AA}$ ,  $d = 100 \text{ \AA}$ , and  $\mathcal{E} = 50 \text{ meV}$ . Panels show results for different NWs: (a) top left reflection, (b) top right, (c) bottom left, and (d) bottom right transmissions. Spin-reversal regions (dark blue) occur for  $\alpha L \simeq L/L_{SO} = \text{constant}$ .

SOI strength,  $\alpha$ , and an applied gate voltage on the bottom right wire,  $V_{g_2}$ . Panels (a) and (c) correspond to the incident energy  $\mathcal{E} = 50 \text{ meV}$ , and panels (b) and (d), to  $\mathcal{E} = 100 \text{ meV}$ . One can see that Fig. 4(a) displays two regions where the  $y$ -polarization is well defined. Around  $\alpha = 0.12 \text{ eV}\cdot\text{\AA}$  and  $V_{g_2} = 0.14 \text{ eV}$  we notice full spin-down polarization, while for the same  $V_{g_2}$  but at  $\alpha = 0.48 \text{ eV}\cdot\text{\AA}$ , one has the opposite polarization. These features change location and sign as the incident energy varies. These results demonstrate the possibility of spin-inversion of the current flux by controlling  $\alpha$  (via  $\mathbf{E}$ ) or  $V_{g_2}$  (via applied gates). Figure 4(c) and (d) correspond to  $T_3$ , and one may note that they present similar behavior, but where features have a smoother (not as sudden) variations in  $\alpha$  or  $V_{g_2}$ .

In conclusion, we have studied the spin transport properties of a nanowire directional coupler implemented by parallel wires joined by a mixing region which generates Rashba spin-orbit interaction (SOI). Using a transfer matrix approach allowed us to understand the modulation of electronic and spin transport arising from the combination of SOI and the system geometrical features. Likewise, SOI and applied gate voltages give rise to a modulation of the polarization when the spin is projected in the same direction as the effective Rashba magnetic field. The versatility of this device may be useful in all-electrical spintronic devices.

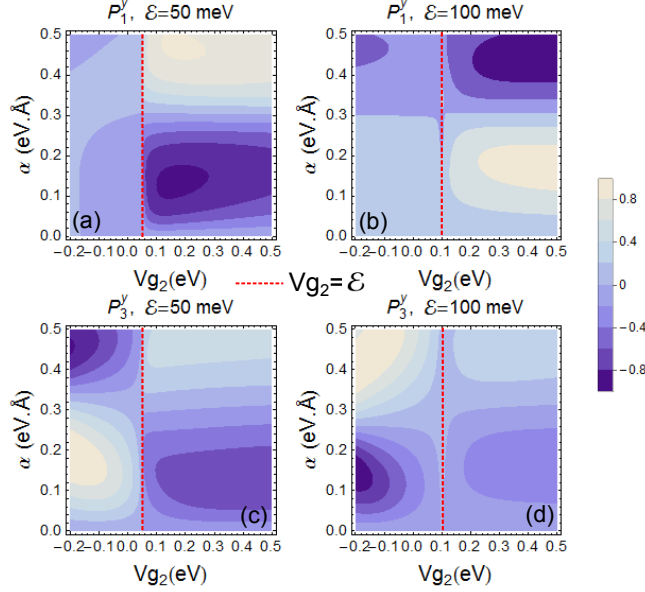


FIG. 4. Polarization in the  $y$ -direction vs  $\alpha$  and applied gate voltage on the bottom right wire, ( $V_{g2}$ ), where  $r_1 = r_2 = 100$  Å,  $d = 100$  Å, and  $L = 300$  nm. (a) Polarization for the top right wire ( $P_1^y$ ) with  $\mathcal{E} = 50$  meV. (b) Polarization for the top right wire ( $P_1^y$ ) with  $\mathcal{E} = 100$  meV. (c) Polarization for the bottom left wire ( $P_3^y$ ) with  $\mathcal{E} = 50$  meV. (d) Polarization for the bottom left wire ( $P_3^y$ ) with  $\mathcal{E} = 100$  meV. Red dashed lines indicate  $V_{g2} = \mathcal{E}$  in each panel.

The authors acknowledge the support of CAPES, CNPQ, and FAPESP-12/02655-1 (Brazil), the Alexander von Humboldt Foundation, and DAAD (Germany), as well as NSF grant 1108285 from DMR-MWM/CIAM (USA).

## REFERENCES

- <sup>1</sup>J. A. del Alamo, and C.C. Eugster, Appl. Phys. Lett. **78**, (1990).
- <sup>2</sup>C. C. Eugster, J. A. del Alamo, M. J. Rooks, and M. R. Melloch, Appl. Phys. Lett. **60**, 642 (1992).
- <sup>3</sup>A. Bertoni, P. Bordone, R. Brunetti, C. Jacoboni, and S. Reggiani, Phys. Rev. Lett. **84**, 5912 (2000).
- <sup>4</sup>S. Datta and B. Das. Appl. Phys. Lett. **56**, 665 (1990).
- <sup>5</sup>O. M. Auslaender, A. Yacoby, R. de Picciotto, K. W. Baldwin, L. N. Pfeiffer, and K. W. West, Science **295**, 825 (2002).
- <sup>6</sup>O. M. Auslaender, H. Steinberg, A. Yacoby, Y. Terkovnyak, B. I. Halperin, K. W. Baldwin, L. N. Pfeiffer, and K. W. West, Science **308**, 88 (2005).



- <sup>7</sup>C. H. L. Quay, T. L. Hughes, J. A. Sulpizio, L. N. Pfeiffer, K. W. Baldwin, K. W. West, D. Goldhaber-Gorson, and R. de Picciotto, *Nature Phys.* **6**, 336 (2010).
- <sup>8</sup>J. C. Egues, G. Burkard, and D. Loss, *Appl. Phys. Lett.* **82**, 2658 (2003).
- <sup>9</sup>L. Zhang, P. Brusheim, and, H. Q. Xu, *Phys. Rev. B* **72**, 045347 (2005).
- <sup>10</sup>S. Nadj-Perge, S. M. Frolov, E. P. A. M. Bakkers, and L. P. Kouwenhoven, *Nature* **468**, 1084 (2010).
- <sup>11</sup>Y. Oreg, G. Rafael, and F. von Oppen, *Appl. Phys. Lett.* **105**, 177002 (2010).
- <sup>12</sup>T. D. Stanescu, R. M. Lutchyn, and S. Das Sarma, *Phys. Rev. B* **87**, 094518 (2013).
- <sup>13</sup>V. Mourik, K. Zuo, S. M. Frolov, S. R. Plissard, E. P. A. M. Bakkers, and L. P. Kouwenhoven. *Science* **336**, 1003 (2012).
- <sup>14</sup>L. P. Rokhinson, X. Liu, and J. K. Furdyna. *Nature Phys.* **8**, 795 (2012).
- <sup>15</sup>P. Debray, S. M. S. Rahman, J. Wan, R. S. Newrock, M. Cahay, A. T. Ngo, S. E. Ulloa, S. T. Herbert, M. Muhammad and M. Johnson, *Nature Nanotech.* **4**, 759 (2009).
- <sup>16</sup>C. Brüne, A. Roth, E. G. Novik, M. Knig, H. Buhmann, E. M. Hankiewicz, W. Hanke, J. Sinova and L.W. Molenkamp. *Nature Phys.* **6**, 448 (2010).
- <sup>17</sup>T.-M. Chen, M. Pepper, I. Farrer, G. A. C. Jones, and D. A. Ritchie. *Phys. Rev. Lett.* **109**, 177202 (2012).
- <sup>18</sup>P. Brusheim, D. Csontos, U. Zülicke, and H. Q. Xu, *Phys. Rev. B* **78**, 085301 (2008).
- <sup>19</sup>E. Rashba, *Fiz. Tverd. Tela (Leningrad)* **2**, 1224 (1960), [*Sov. Phys. Solid State* **2**, 1109 (1960)].
- <sup>20</sup>F. Zhai and H. Q. Xu, *Phys. Rev. Lett.* **94**, 246601 (2005).
- <sup>21</sup>R. Tsu, and L. Esaki, *Appl. Phys. Lett.* **22**, 562 (1973).
- <sup>22</sup>U. Zülicke and C. Schroll, *Phys. Rev. Lett.* **88**, 029701 (2002).
- <sup>23</sup>D. Boese, M. Governale, A. Roch, and U. Zülicke, *Phys. Rev. B* **64**, 085315 (2001).
- <sup>24</sup>E. Bielejec, J. A. Seamons, J. L. Reno, and M. P. Lilly, *Appl. Phys. Lett.* **86**, 083101 (2005).
- <sup>25</sup>B. K. Nikolić, and S. Souma, *Phys. Rev. B* **71**, 195328 (2005).